JACS Au
AN OPEN ACCESS JOURNAL OF THE AMERICAN CHEMICAL SOCIETY

Open Access
This article is licensed under CC-BY-NC-ND 4.0

pubs.acs.org/jacsau
Article

Co-upcycling of Plastic Waste and Biowaste via Tandem Transesterification Reactions

Jiaquan Li, Xingmo Zhang, Xingxu Liu, Xiuping Liao, Jun Huang,* and Yijiao Jiang*

Cite This: JACS Au 2024, 4, 3135−3145

Read Online

ACCESS | Metrics & More | Article Recommendations | Supporting Information

ABSTRACT: Polyethylene terephthalate (PET) and glycerol are prevalent forms of plastic and biowaste, necessitating facile and effective strategies for their upcycling treatment. Herein, we present an innovative one-pot reaction system for the concurrent depolymerization of PET plastics and the transesterification of glycerol into dimethyl terephthalate (DMT), a valuable feedstock in polymer manufacturing. This process occurs in the presence of methyl acetate (MA), a byproduct of the industrial production of acetic acid. The upcycling of biowaste glycerol into glycerol acetates renders them valuable additives for application in both the biofuel and chemical industries. This integrated reaction system enhances the conversion of glycerol to acetins compared with the singular transesterification of glycerol. In this approach, cost-effective catalysts, based on perovskite-structured $CaMnO_3$, were employed. The catalyst undergoes in situ reconstruction in the tandem PET/glycerol/MA system due to glycerolation between the metal oxides and glycerol/acetins. This process results in the formation of small metal oxide nanoparticles confined in amorphous metal glycerolates, thereby enhancing the PET depolymerization efficiency. The optimized coupled reaction system can achieve a product yield exceeding 70% for glycerol acetates and 68% for PET monomers. This research introduces a tandem pathway for the simultaneous upcycling of PET plastic waste and biowaste glycerol with minimal feedstock input and maximal reactant utilization efficiency, promising both economic advantages and positive environmental impacts.

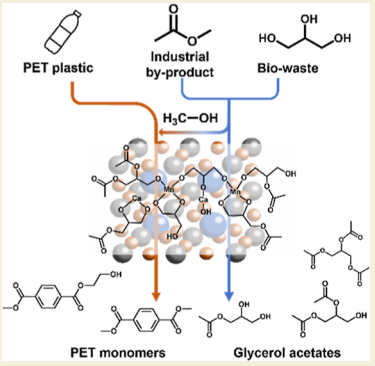

KEYWORDS: *PET, glycerol, co-upcycling, tandem reaction, metal glycerolate, transesterification*

INTRODUCTION

With the escalating demand for plastic production and its widespread daily use, urgently addressing global white pollution requires a focused effort on plastic waste recycling.[1,2] Despite the substantial annual production of plastic waste, only 9% undergoes successful recycling.[3] Polyethylene terephthalate (PET), a common polyester plastic extensively employed in food packaging, drink containers, and textiles, constitutes 13% of the total plastic production and is a key contributor to this waste stream.[4] Presently, PET waste is predominantly processed through mechanical recycling, involving melting and physical transformation, without inducing any chemical structure changes. However, this method unavoidably leads to deterioration of the properties and lower quality of PET products. In this context, chemical upcycling of PET waste into depolymerized aromatic monomers or higher-value chemicals is a more attractive recycling strategy. Various methods have been explored for the valorization of PET waste,[5,6] including hydrogenolysis,[7−9] solvolysis,[10,11] pyrolysis,[12] photocatalytic[13,14] and electrochemical upcycling,[15] and hybrid processes.[16−19] However, most of these methods require additional inputs of valuable chemicals and energy resources, such as H_2, alcohols, intensive heat, and electricity.

Solvolysis is a method extensively studied for addressing polyester plastic waste, with glycolysis and methanolysis standing out as the two representative approaches that have received the most attention. Methanolysis is a transesterification process to decompose PET into dimethyl terephthalate (DMT) and ethylene glycol (EG) by solvolysis with methanol.[20] Compared to the glycolysis process, the final product DMT from methanolysis of PET is more convenient to purify due to its low solubility in water. DMT serves as a feedstock for synthesizing polyester plastics, resins, films, and paint, or as a valuable additive in polymer manufacturing.[21] Its global price has fluctuated between 900 and 1300 US dollars per metric ton (USD/mt) over the past 5 years.[22] Current methodologies for PET methanolysis can be categorized into two main approaches: supercritical reactions, endowed at high temperatures exceeding 250 °C and elevated pressures,[23,24] and catalytic methanolysis, which effectively mitigates the need for extreme conditions by lowering both the reaction temperature and pressure.[25]

Received: May 29, 2024
Revised: July 16, 2024
Accepted: July 23, 2024
Published: July 30, 2024

© 2024 The Authors. Published by American Chemical Society

https://doi.org/10.1021/jacsau.4c00459
JACS Au 2024, 4, 3135−3145

The commonly used catalysts for PET methanolysis include homogeneous catalysts such as metal acetates,[26] heterogeneous transition-metal and alkali earth metal oxides,[27] and metal-free ionic liquids.[28] The homogeneous catalysts may cause product purification problems. Catalytic methanolysis was observed to proceed through the interaction between the transition-metal cation M^{n+} center and the carbonyl groups within PET, resulting in the enhanced activation of the O−H bond in methanol.[25] It has also been reported for alkali earth metal catalysts; methanol is first activated by M^{2+} to form M−O−CH_3 which further reacts with the ester groups in PET.[27] However, in heterogeneous catalysis, the limited dispersion of catalytically active sites poses a challenge, impeding their efficient contact with reactants, particularly polymers. There is a need to augment the effective interaction between catalytic sites and PET. It is worth noting that while both alkali earth metal catalysts (e.g., MgO and CaO) and transition-metal catalysts (e.g., Mn_3O_4, Fe_3O_4, and ZnO) have been investigated for the alcoholysis of PET,[25,27,29−32] there has been limited exploration into enhancing catalytic performance by combining two or more metal oxides, leveraging the benefits of a synergistic catalytic mechanism. Moreover, a high methanol/PET ratio is required to improve the overall methanolysis efficiency, which needs a large amount of methanol loading. Given methanol's crucial role as a fuel source, solvent, and building block in the contemporary chemical industry, obtaining methanol from less valued industrial wastes or byproducts, such as biomass wastes, would be a more favorable and sustainable approach.

Glycerol, derived from biomass, undergoes extensive industrial production, constituting approximately 10% of the byproducts generated during biodiesel manufacturing.[33,34] The burgeoning production of biodiesel has spurred a rise in glycerol output, resulting in oversaturation and a subsequent price decline. Presently, glycerol production has exceeded market capacity, rendering it a biowaste. Projections indicate that biodiesel production will reach 60 billion liters by 2025, yielding approximately 6 billion liters of glycerol biowaste.[35] Consequently, urgent efforts are needed to devise efficient methods for glycerol valorization before it becomes a pollutant. Glycerol's inherent reactivity, attributed to its three hydroxyl groups, positions it as a highly promising precursor for the synthesis of diverse value-added products.[36]

An attractive approach to upgrade glycerol is to convert it into glycerol esters by esterification or transesterification.[37−40] For instance, the acetylation of glycerol can produce glycerol acetates (acetins) as valued chemicals in diverse applications with increasing market demands. Acetins including monoacetin, diacetin, and triacetin are widely used for cosmetics, pharmaceuticals, food additives, and biodiesel additives.[41] The average price of glycerol stands at 350 USD/mt, but its conversion into acetins can elevate its value significantly, ranging from 1000 to 2000 USD/mt.[42,43] The conversion of glycerol into acetins can be achieved through the transesterification of glycerol with methyl acetate (MA), a byproduct extensively generated in the manufacturing process of poly(vinyl alcohol) (PVA).[44] The worldwide annual production of PVA is over 1 Mt, leading to the generation of 1.68 Mt MA, suggesting a promising alternative solution for the downstream utilization of glycerol.[45] The transesterification of glycerol and MA has been reported in several research papers using acid-modified silica, silica-supported yttrium, and lipase catalysts.[45−47] However, a comprehensive investigation into the reaction performance utilizing metallic catalysts is still pending. In addition to the three glycerol acetate products, methanol is generated as a byproduct from the transesterification of glycerol and MA. This observation opens up the possibility of synergizing the transesterification processes of glycerol, MA, and PET plastics. The methanol produced in the reactions between glycerol and MA can potentially act as a reactant in the methanolysis of PET.

In this work, a one-pot reaction system simultaneously managing PET plastic, MA, and glycerol via tandem transesterification is reported. In this process, all of the reactants are wastes with low costs, and the valorization occurred via the internal reactions among the three wastes with no additional feedstocks such as methanol needed. The industrial biowaste glycerol is valorized into glycerol acetates (mono-, di-, and triacetin) in the reaction with MA; meanwhile, the coproduct methanol allows methanolysis for the depolymerization of PET plastics into oligomers, then 2-hydroxyethyl methyl terephthalate (HEMT), and finally the DMT monomers, as illustrated in Scheme 1. Alkali earth-metal and transition-metal catalysts were screened in this work, which presented dual activity in the two tandem transesterification reactions. Moreover, it was found that the perovskite-type $CaMnO_3$ catalyst underwent in situ reconstruction during the tandem reactions within the PET/glycerol/MA system. This transformation occurred due to glycerolation between the metal and glycerol/acetins, resulting in the formation of small metal oxide nanoparticles confined within amorphous metal glycerolates. This newly formed structure exhibits exceptional activity for the depolymerization of PET to DMT monomers. This work demonstrates the co-upcycling of plastic waste and industrial biowaste to maximize the feedstock utilization efficiency and attain higher sustainability.

Scheme 1. Tandem Transesterification Reactions of MA, Glycerol, and PET Proposed in This Work

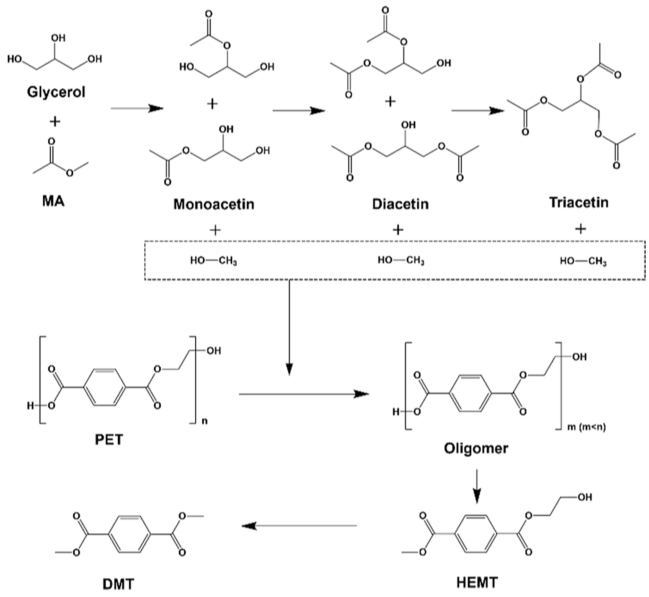

RESULTS AND DISCUSSION

A transparent PET film with the size of 5 mm × 5 mm was used in this work as shown in the image in Figure S1A. Diffraction peaks at 2θ = 23.2 and 26.0° with hkl values of

https://doi.org/10.1021/jacsau.4c00459
JACS Au 2024, 4, 3135−3145

(110) and (100), respectively, were identified for the PET crystalline structure, as shown in Figure S1B. Since the two proposed subreactions in this study involve transesterification, the catalyst screening began with the catalysts that could potentially be applied in both processes. We selected alkali earth metals Ca and Mg, as well as transition metal Mn, as the starting materials to develop a range of metal-based catalysts with diverse structures and compositions including Ca- and Mg-based catalysts [CaO, MgO, Ca, and Mg layered double hydroxide (LDH)] and Mn-based catalyst (MnO_x). Furthermore, a $CaMnO_3$ perovskite oxide was synthesized to investigate the performance of a dual-metal catalyst containing both alkaline earth and transition metals. Prior to the coupled tandem reaction, the catalysts were first tested in two individual transesterification reactions, namely, glycerol acetylation and PET methanolysis. As depicted in Figure 1A,

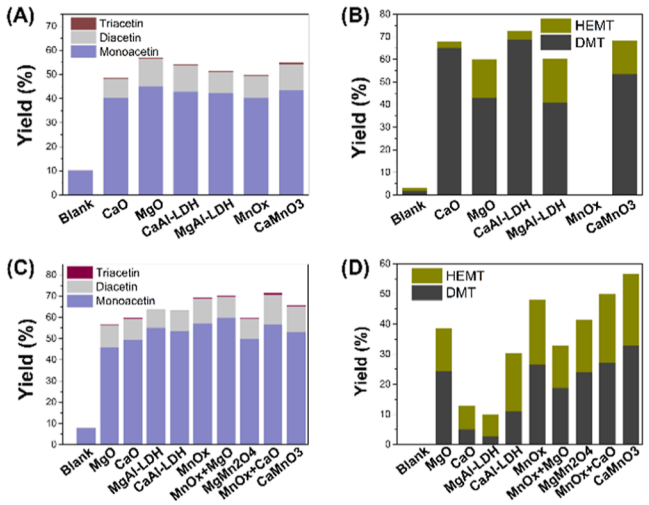

Figure 1. Reaction behavior of different catalysts in (A) transesterification with MA and glycerol (GM reaction); (B) methanolysis of PET with methanol; (C,D) tandem reaction of glycerol, MA, and PET (PGM reaction). Reaction conditions: (A) 10 mmol of glycerol, 30 mmol of MA, 2 mL of 1,4-dioxane, 200 °C, 5 h, 1 atm argon. (B) 2 mL of 1,4-dioxane, 2 mL of methanol, 0.3 g of PET film, 200 °C, 2 h, 1 atm argon. (C,D) 10 mmol of glycerol, 30 mmol of MA, 2 mL of 1,4-dioxane, 0.05 g of PET film, 200 °C, 7 h, 1 atm argon. 1.8 mmol of the catalyst was loaded according to its chemical formula. For combined catalysts, 3.6 mmol of MnO_x and 1.8 mmol of MgO were loaded to achieve the same metal loading as $MgMn_2O_4$ spinel oxides, and 1.8 mmol of MnO_x and 1.8 mmol of CaO were loaded to achieve the same metal loading as $CaMnO_3$.

the transesterification of glycerol and MA without PET (referred to as the GM reaction) was carried out with a stoichiometric molar ratio of MA/glycerol = 3 at 200 °C for 5 h. Compared to the catalyst-free test, all the adopted catalysts exhibited remarkable activity, enhancing the product yield by at least 4-fold. There is minimal disparity in the activities of the Ca, Mg, and Mn catalysts, suggesting that the GM reaction is readily catalyzed by a diverse array of catalysts. The compositions of the glycerol acetate products are also similar among different catalysts. Due to the stoichiometric dosage of MA and glycerol, monoacetin constitutes the largest portion of the products, followed by diacetin, with triacetin being the least abundant among the three. Previous studies have utilized an excess of MA relative to glycerol to enhance the yield of triacetin.[45] However, this approach represents a trade-off between the cost of feedstock and the desired product yield.

The catalytic performance was then monitored in the methanolysis reaction of PET with excess methanol loading at 200 °C for 2 h. The reaction efficiency was assessed based on the yields of two monomers resulting from PET depolymerization. These monomers, containing a single aromatic ring in their molecules, can be purified and serve as feedstocks for the repolymerization process with EG to regenerate high-quality PET plastics. The yields of both DMT and HEMT are depicted in Figure 1B. The degradation of PET barely occurred without a catalyst, while all the Ca- and Mg-containing catalysts afforded a high yield of DMT, with the Ca-based catalyst showing superior activity against the Mg-based ones to yield DMT close to 70% over CaAl-LDH. It is possibly due to the stronger basicity of Ca to activate the O−H bond of methanol. However, the formation of DMT and HEMT was scarcely observed over MnO_x, indicating its inactivity for PET methanolysis. It is worth mentioning that $CaMnO_3$ exhibited lower activity compared to that of CaO and CaAl-LDH, despite containing an identical amount of Ca. This suggests that the composite catalyst formed by $CaMnO_3$ hindered the methanolysis efficiency of PET.

The feasibility of applying the catalytic system into the designed tandem transesterification of glycerol, MA, and PET (referred to as PGM reaction) was explored afterward at 200 °C for 7 h without the loading of methanol, and the product yields of glycerol acetate and DMT/HEMT are displayed in Figure 1C,D, respectively. The distribution of the glycerol acetate products in PGM reactions is similar to that in GM reactions over different catalysts. The monoacetin yield fell into a range between 45 and 60% for all the catalysts. MnO_x shows slightly higher overall product yields compared to the Ca- and Mg-based catalysts, which contrasts with the GM reaction shown in Figure 1A. This suggests that MnO_x boosted the performance of glycerol acetylation in the tandem reaction system. The PET depolymerization efficiency in this tandem reaction is reasonably lower than that in direct methanolysis by methanol due to the lower methanol concentration generated from the reaction between MA and glycerol. Interestingly, MnO_x achieved higher DMT and HEMT yields than MgO, despite its inactivity in PET methanolysis, as shown in Figure 1B. It is conceivable that new catalytically active species were generated during the PGM process, rendering it capable of catalyzing the depolymerization of PET with the in situ-formed methanol. This phenomenon will be further explored in the upcoming mechanism studies.

The highest yields of DMT (32.8%) and HEMT (23.9%) were attained over $CaMnO_3$, indicating that the combined presence of Ca and Mn in a single catalyst surpasses the performance of individual metal oxides of Ca and Mn. For comparison, the combination of Mg and Mn in the form of a single catalyst, namely, $MgMn_2O_4$ spinel oxides, was also evaluated in the PGM tandem reaction. However, the PGM reaction performance of $MgMn_2O_4$ spinel oxides is inferior to that of both MgO and MnO_x, suggesting that the catalytic efficacy in PGM is influenced by the composition and structure of the mixed oxides, rather than the simple accumulation of each metal component. For further comparison, we tested the PGM reaction with both MnO_x and CaO to achieve identical loading of Ca and Mn as $CaMnO_3$. The product yield of this MnO_x/CaO mixture is slightly higher than that of MnO_x but still lower than that of $CaMnO_3$. This indicates that the

https://doi.org/10.1021/jacsau.4c00459
JACS Au 2024, 4, 3135−3145

$CaMnO_3$ catalyst outperforms each individual metal component and its simple combination. Furthermore, the coexistence of both MnO_x and MgO for PGM resulted in even poorer performance than the individual catalysts, indicating a negative effect of this dual-catalyst configuration. We speculate that this could possibly be attributed to the strong association of methanol with MgO, which inhibited effective interaction with Mn-based active sites to effectively react with PET since MgO and MnO_x are separated particles. Therefore, $CaMnO_3$ is considered as the best catalyst in this tandem reaction system, where the activity does not simply accumulate from Ca and Mn. It was chosen as the representative catalyst for subsequent studies.

To monitor the reaction process, track the evolution of product formation, and assess the impact of PET presence on the GM reaction efficiency, we utilized $CaMnO_3$ as the catalyst and conducted both the GM and PGM reactions individually for a duration of 20 h. The GM and PGM reactions were conducted under the same conditions except for the PET loading in PGM. As depicted in Figure 2A, the monoacetin yield reached 41% at 2.5 h in the GM reaction, which is identical to that observed in the PGM reaction. Subsequently, the product yield gradually increased over time, ultimately reaching 65% at the 20 h mark, with a cumulative 78% yield attained for all three glycerol acetate products in the GM reaction. In the PGM reaction, the productivity surpassed that of the GM reaction for all three glycerol acetate products. Notably, final yields of 80 and 98% were achieved for monoacetin and total products, respectively, in the PGM reaction at 20 h. Hence, it can be inferred that the glycerol acetylation process is enhanced in the presence of PET, potentially attributed to the consumption of in situ-produced methanol, leading to a shift in the reaction equilibrium toward greater product formation.

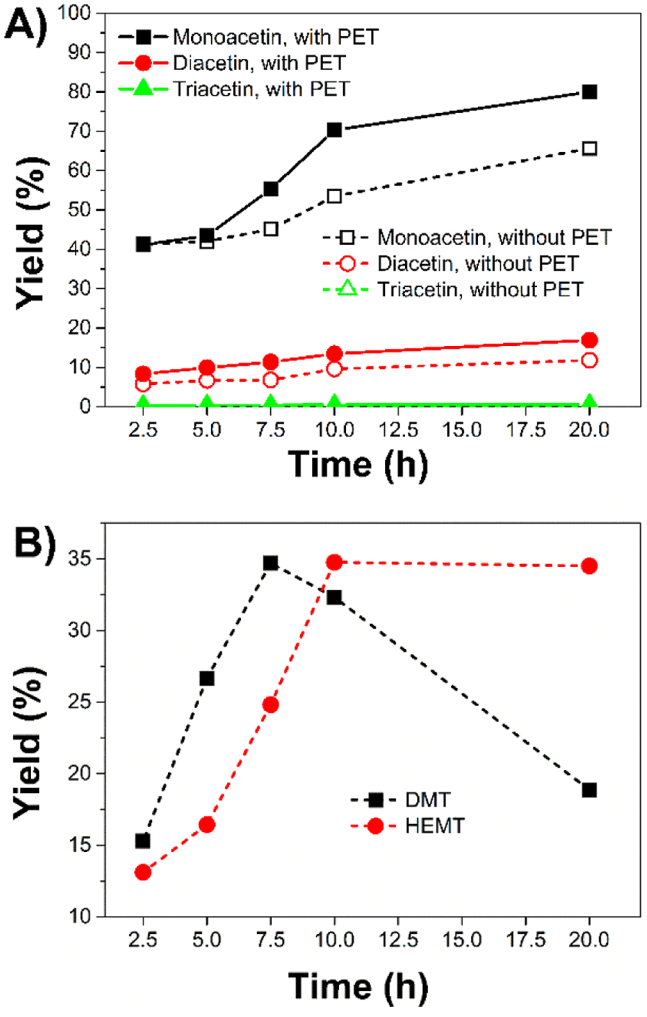

Figure 2. Comparison of the product evolution with reaction time for the GM (without PET) and PGM (with PET) reactions. (A) Glycerol acetate yields in the GM and PGM reactions. (B) DMT/HEMT yields in the PGM reaction. Conditions: 10 mmol of glycerol, 30 mmol of MA, 2 mL of 1,4-dioxane, 0.025 g of PET film, 200 °C, catalyst: 1.8 mmol of $CaMnO_3$.

The evolution of DMT and HEMT product yield in the PGM reaction is presented in Figure 2B. After 2.5 h of tandem reaction, 15.3% DMT and 13.1% HEMT were achieved. The DMT yield peaked at 7.5 h, reaching 34.7%, before gradually declining. Conversely, the HEMT yield continued to rise until 10 h of reaction and then reached a plateau of 34.5%. This phenomenon can be understood through the following interpretations: initially, the methanolysis of PET occurs at random points along the PET chain, leading to the production of oligomers. Subsequently, chain shortening ensues, resulting in the formation of HEMT which contains a single aromatic ring with one side chain remaining to be released through the transesterification by methanol. Afterward, HEMT is ultimately transformed into DMT. However, after 7.5 h of reaction time, the concentration of DMT reaches its peak, signifying the onset of enhanced and dominant repolymerization. DMT reacts with EG to form HEMT and continues to undergo further polymerization, leading to the formation of longer chains. Consequently, the decrease in DMT yield after 7.5 h can be attributed to this enhanced repolymerization process, while HEMT exhibits negligible change due to the coexistence of depolymerization and repolymerization. Similar repolymerization results were also observed in the previously reported research on PET degradation by methanolysis and glycolysis.[27,48]

The influence of the reaction conditions was also investigated on the $CaMnO_3$ catalyst to gain a comprehensive understanding of the PGM reaction process. As shown in Figure S2A,B, the reaction temperature presented a significant influence on the yield of products, especially the PET degradation. Both the yields of glycerol acetates and DMT/HEMT increased with elevated temperature. At 170 °C, 36% monoacetin and 10% diacetin were gained, which were gradually increased to 53 and 12%, respectively, at 200 °C. Nevertheless, the DMT yield was only 0.5 and 5.7% at 170 and 180 °C, respectively. At higher temperatures of 190 and 200 °C, the yield of DMT and HEMT was remarkably enhanced. This indicates that the glycerol acetylation subreaction requires lower activation energy than PET depolymerization into DMT.

The impact of the loading amount of $CaMnO_3$ on the PGM process was studied as summarized in Figure S2C,D. The increment of catalyst loading from 0.45 to 0.9 and 1.8 mmol resulted in a noticeable increase in glycerol acetates and PET monomers at a similar scale, attributed to the multiplication of catalytic sites dedicated to the reaction. However, upon further increasing the $CaMnO_3$ dosage to 3.6 mmol, no significant increase in the glycerol acetate products was observed. Instead, there was a slight decrease in DMT yield and a substantial increase in HEMT. This could be explained by the equilibrium

https://doi.org/10.1021/jacsau.4c00459
JACS Au 2024, 4, 3135−3145

of the transesterification caused by excess catalyst loading when the DMT started to convert into HEMT by EG. The highest DMT + HEMT yields of 68% were observed at a $CaMnO_3$ dosage of 3.6 mmol. Notably, no PET residual was observed in the product solution after the reaction, indicating that all of the PET was depolymerized into soluble oligomers and monomers.

Furthermore, the solvent 1,4-dioxane was removed or substituted with other solvents to investigate its role in $CaMnO_3$-catalyzed PGM. The results are illustrated in Figure S3. Compared to PGM with 1,4-dioxane, the removal of the solvent led to a dramatic decrease in DMT yield from 32.8 to 7%. The solvent's role could be identified as facilitating the dissolution of short-chain PET molecules, allowing better contact with the catalyst and methanol to form DMT and HEMT. Additionally, three other solvents including toluene, dichloromethane, and chloroform were also tested. The reaction efficiency over different solvents followed the sequence of 1,4-dioxane > chloroform > dichloromethane > toluene > solvent-free. Thus, 1,4-dioxane emerged as the superior solvent in this PGM system.

Meanwhile, the composition of the three feedstocks was adjusted individually to see the influence on the reaction yield. The results are summarized in Table S1. When the MA loading was doubled from the reference of 10 mmol of glycerol, 30 mmol of MA, and 0.05 g of PET film, a decrease in monoacetin, DMT, and HEMT yields by 16, 21, and 11% respectively, was observed. This reduction may be attributed to the decreased solubility of PET oligomers with a higher portion of MA. Similarly, doubling the glycerol in the PGM system also resulted in reduced product yields. It is noted that the high loading of glycerol could not fully dissolve into the reaction solution, and the metal oxide catalyst exhibited a higher affinity toward glycerol, becoming confined to the glycerol phase. This weakened the interaction between the catalyst and the PET/methanol reactants. Additionally, when the PET dose was reduced by 50%, there was no significant variation in the product yield, indicating that the PET methanolysis equilibrium is not greatly shifted, as glycerol/MA is excessive compared to PET.

The influence of the specific surface area (SSA) of the $CaMnO_3$ catalyst was also studied in this work. In addition to the sol−gel preparation method, coprecipitation and hydrothermal methods were employed to prepare $CaMnO_3$ catalysts with varying SSA. The SSA of the catalysts follows the sequence hydrothermal > sol−gel > coprecipitation, as summarized in Table S2. However, no clear correlation between the catalytic performance in the PGM reaction and the SSA was observed (Figure S4). Specifically, the three catalysts produced similar yields of acetins, while $CaMnO_3$ (sol−gel) delivered a slightly higher DMT yield than those prepared by coprecipitation and hydrothermal methods. This indicates that the SSA of the catalyst is not the primary factor influencing the catalytic activity.

The mass balance and carbon balance were calculated in the PGM reaction with $CaMnO_3$. The calculation method is described in the Experimental Section. The total mass balance of this system is calculated to be 96.0% (Figure S5A). The loss of mass balance was possibly due to the reacted glycerol species with the catalyst and the mass loss during chemical transfer. The carbon balance, calculated from all the detected components excluding the PET oligomers, was found to be 91.6% (Figure S5B).

As previously mentioned, there may be the generation of new catalytic sites over the MnO_x catalyst during PGM reactions for PET depolymerization. This is evidenced by the shift observed in MnO_x from being inactive in PET methanolysis to becoming active in PGM. To elucidate the key component contributing to the transition of MnO_x, MnO_x was pretreated in various environments. Subsequently, the MnO_x catalysts were collected by filtration, rinsed with 1,4-dioxane, and evaluated in a PET/methanol reaction system. Five different treatment environments were employed on MnO_x at 200 °C for 7 h: (1) 1,4-dioxane solvent only; (2) MA + solvent; (3) glycerol + solvent; (4) GM reaction environment; (5) PGM reaction environment. The results are presented in Figure 3A.

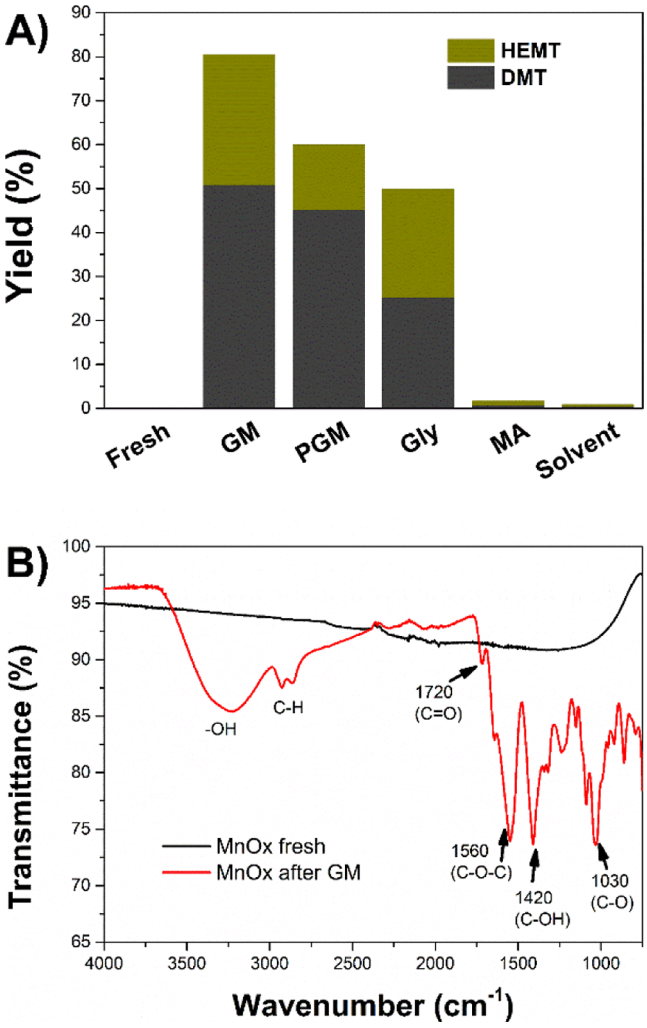

Figure 3. (A) PET methanolysis over MnO_x catalysts after different pretreatments. The treatments include (1) 1,4-dioxane (solvent); (2) MA + solvent (MA); (3) glycerol + solvent (Gly); (4) GM reaction environment; (5) PGM reaction environment. (B) FTIR spectra of fresh MnO_x and MnO_x after the GM reaction.

For the PET methanolysis conducted on untreated MnO_x and MnO_x treated with (1) and (2), the overall DMT + HEMT yield was lower than 2%, indicating that no active sites were generated. The DMT and HEMT yield was substantially improved over the MnO_x treated by (3), (4), and (5), suggesting that the interaction between MnO_x and glycerol

https://doi.org/10.1021/jacsau.4c00459
JACS Au 2024, 4, 3135−3145

played a crucial part in the generation of new active sites. It has been reported that glycerol can form associations with a variety of metals due to its abundant hydroxyl groups, leading to the formation of metal glycerolates (*M*-glycerolates).[49] These compounds significantly enhance the exposure of metal sites, making them accessible for catalytic reactions. Transition metals such as Zn, Mn, Fe, Co, and Ni are known to readily associate with glycerol in this manner.[50,51] Moreover, recent research has unveiled a significant discovery regarding PET glycolysis, revealing that the Zn catalyst has the capability to engage with EG, leading to the formation of Zn-glycolate species.[48] These species have been proven to be efficient catalytic agents in the degradation of PET via glycolysis. Drawing inspiration from this observation, we hypothesize that during the GM reaction, glycerol can similarly interact with MnO_x to produce Mn-glycerolate species, which exhibit catalytic activity in the methanolysis of PET with enhanced accessibility to PET flakes.

To verify the successful glycerolation of MnO_x, the surface chemical bonds of MnO_x after GM treatment were analyzed by using Fourier transform infrared (FTIR) spectra within the wavelength range of 500−4000 cm^{-1}. As depicted in Figure 3B, no distinct peaks were detected on fresh MnO_x, while signals corresponding to alkyl chains and OH group vibrations appeared in the spectral regions at 2930 and 3380 cm^{-1}, respectively. Peaks at 1720, 1560, and 1420 cm^{-1} are assigned to C═O, C−O−C, and C−OH, respectively,[52] indicating the association of the MnO_x catalyst with both glycerol and glycerol acetates. X-ray diffraction (XRD) analysis of fresh MnO_x revealed strong patterns of Mn_2O_3 and MnO_2 (Figure S6). Following GM treatment, the peaks for Mn_2O_3 and MnO_2 nearly vanished, consistent with the existing literature, suggesting the transformation of the crystalline structure of metal-based materials into an amorphous state due to the formation of *M*-glycerolates.[53] Specifically, the XRD data in Figure S6 indicate that after the reaction, the Mn_2O_3 signals became higher and sharper than the MnO_2 signals. To gain a better understanding of this phenomenon, XPS Mn 2p spectra of MnO_x before and after the reaction were analyzed. The results in Figure S7 suggested that the ratio of Mn^{3+}:Mn^{4+} for reacted MnO_x (1.47) was slightly lower than that of fresh MnO_x (1.50). As the decrease and broadening of the XRD signal are due to the generation of amorphous Mn-glycerolate species, we conjectured that this could possibly be because the Mn^{4+} cations with higher valence state are more active than Mn^{3+} in associating with the O atoms to form Mn-glycerolate. Consequently, Mn^{4+} became amorphous on the surface of the catalyst, leading to a broadened XRD signal but a higher XPS proportion than Mn^{3+}.

Furthermore, we performed GM treatment for CaO and $CaMnO_3$, with the FTIR spectrum demonstrating analogous peaks of the fresh and GM-treated samples as shown in Figure 3B, suggesting that CaO and $CaMnO_3$ can also generate *M*-glycerolate species (Figure S8). Notably, Figure 3A illustrates that the yields of DMT and HEMT from GM-treated MnO_x surpassed those from glycerol alone, leading us to infer that under GM and PGM reaction conditions, Mn interacts with both glycerol and glycerol acetates to form mixed Mn-glycerolate species that serve as the boosted active sites for PET depolymerization.

The reusability of $CaMnO_3$ in PGM reactions was tested in four cycling runs. The characterization of the filtered catalyst also shed light on the new active site generation over $CaMnO_3$ during the PGM reaction. Following the PGM reaction, the initial black $CaMnO_3$ powder transitioned to a brown hue, as depicted in Figure S6A,B. To investigate the structure evolution of the catalyst during the cycling runs, both the fresh and the spent catalysts were characterized by XRD, TG analysis, X-ray photoelectron spectroscopy (XPS), and scanning electron microscopy (SEM) imaging. The XRD spectrum of the fresh catalyst displayed typical patterns of $CaMnO_3$ structures indexed to the orthorhombic perovskite, in accordance with the standard card,[54−56] while after the PGM reaction, these signals nearly vanished (Figure 4A), aligning

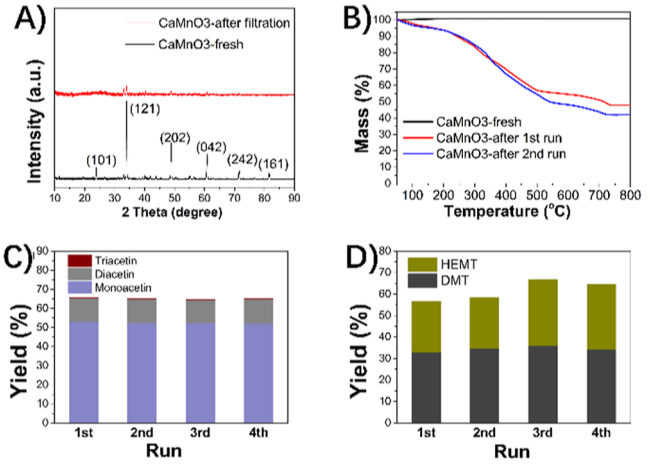

Figure 4. (A,B) Reusability test of $CaMnO_3$ in the PGM reaction for 4 runs. Conditions: 10 mmol of glycerol, 30 mmol of MA, 2 mL of 1,4-dioxane, 0.05 g of PET film, 200 °C, 7 h, catalyst loading: 1.8 mmol of $CaMnO_3$. (C) XRD patterns of fresh and used $CaMnO_3$. (D) TGA of fresh and used $CaMnO_3$.

with the results observed for MnO_x (Figure S6), thus confirming the formation of amorphous *M*-glycerolates on $CaMnO_3$. The mass of the filtered catalyst after the reaction was higher than that of the loaded fresh catalyst due to the generated *M*-glycerolates. TGA conducted in air to determine the formed organic species on the catalyst revealed continuous weight loss for $CaMnO_3$ after the first run until reaching 735 °C, with a total weight loss of 52.1%, contrasting the absence of weight loss on fresh $CaMnO_3$ (Figure 4B). After the second run, the $CaMnO_3$ catalyst demonstrated an even greater weight loss, reaching 58.1%. This observation indicates that the continuous formation of metal glycerolates occurred during the tandem reaction. For the cycling experiment, the used catalyst underwent filtration, washing with 1,4-dioxane, and drying for subsequent use. Since the weight of the catalyst increased after the reaction, the mass loading of the catalyst for the next cycling run was recalculated based on the TGA results to ensure consistent loading of metal content with the former cycling run. As illustrated in Figure 4C,D, the four cycling runs exhibited no discernible loss of activity in producing glycerol acetates and PET monomers. Specifically, the production of glycerol acetates remained almost unchanged throughout the cycles. During the PET depolymerization, the production of monomers exhibited a slight increase in the third and fourth runs, potentially attributed to the in situ generation of catalytically active species. This underscores the excellent reusability of the $CaMnO_3$ catalyst in facilitating this tandem reaction. We also conducted inductively coupled plasma-optical emission spectrometry (ICP-OES) to detect the metal

https://doi.org/10.1021/jacsau.4c00459
JACS Au 2024, 4, 3135−3145

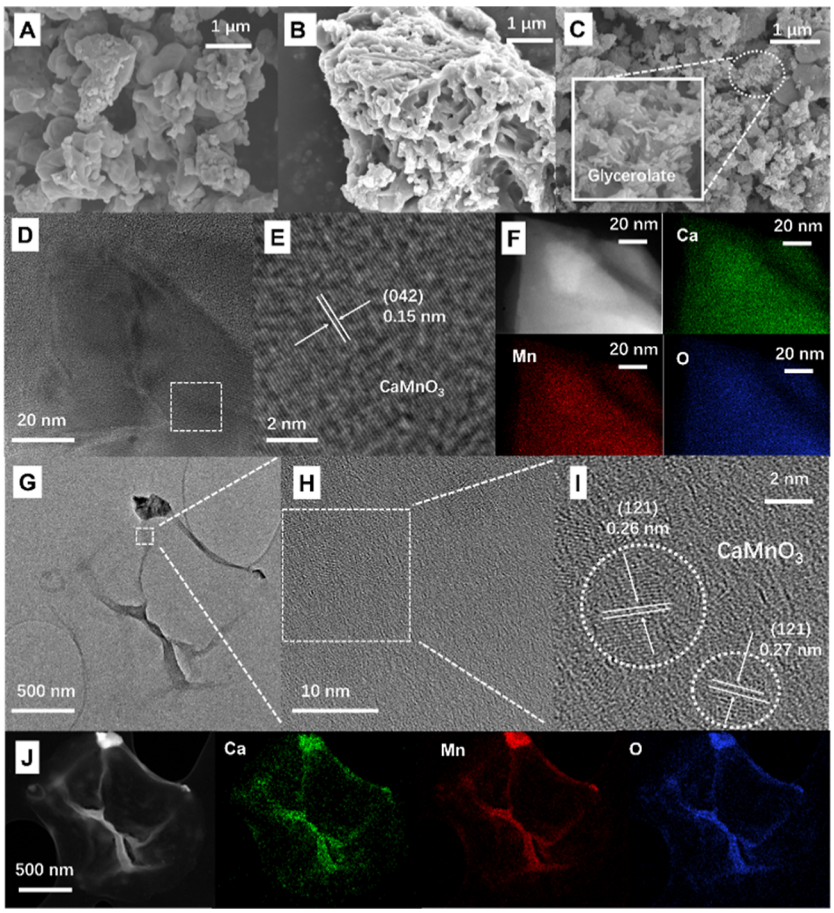

Figure 5. (A−C) SEM images of $CaMnO_3$: (A) fresh sample. (B,C) filtered samples after the first and third run of the PGM reaction, respectively. HR-TEM images (D,E) and STEM and EDS mapping (F) of the fresh $CaMnO_3$ catalyst. TEM (G), HR-TEM (H−I), and STEM and EDS mapping (J) of the filtered $CaMnO_3$ catalyst after the PGM reaction.

leaching within the filtered reaction solution after the catalytic reaction. Only a trace amount of the Mn cation was detected in the product solution from the fresh catalyst. This trace amount of Mn leaching possibly originated from the surface defect sites on the catalyst generated during the catalyst preparation. Considering the excellent catalytic performance during the cycling runs, it can be inferred that there was no loss of active-metal sites during the reaction.

SEM images of fresh $CaMnO_3$ and $CaMnO_3$ after the first and third runs depict morphological changes in the catalyst during the cycling test (Figure 5A−C). Compared to the fresh $CaMnO_3$, the surface of catalyst particles exhibited slight roughening after the first run due to the presence of glycerolates (Figure 5A,B). Following the third run, metal glycerolates accumulated, forming small flakes on the catalyst (Figure 5C). The high-resolution transmission electron microscopy (HR-TEM) images of fresh $CaMnO_3$ revealed a uniform lattice structure of the $CaMnO_3$ phase (Figure 5D,E). Scanning transmission electron microscopy (STEM) and energy-dispersive X-ray spectroscopy (EDS) mapping in Figure 5F further corroborated the formation of the $CaMnO_3$ structure, demonstrating an even dispersion of Ca, Mn, and O throughout the catalyst. The TEM image of the filtered catalyst after the PGM reaction (Figure 5G) exhibited the formation of metal-glycerolate flakes due to the reaction between $CaMnO_3$ and glycerol. The HR-TEM images in Figure 5H,I reveal that the filtered catalyst exhibits an amorphous structure with crystal nanoparticles dispersed randomly, each averaging several nanometers in size. STEM and EDS mappings in Figure 5J indicate the widespread dispersion of both Ca and Mn throughout the flakes, confirming the formation of metal-glycerolate species. This observation suggests that during the tandem reaction, glycerol and acetins reactively decompose the $CaMnO_3$ catalyst, resulting in the formation of amorphous metal-glycerolate flakes that encapsulate small $CaMnO_3$ nanoparticles, in accordance with the XRD results. The XPS O 1s spectra were deconvoluted into three main species, namely, Mn−O−C (533.2 eV), lattice oxygen (530.7 eV), and adsorbed oxygen (527.5 eV). Deconvolution of the XPS O 1s spectra unveiled a significant decrease in lattice oxygen on the fresh $CaMnO_3$ following the tandem reaction. This decline was accompanied by an increase in M−O−C species (Figure 6), providing further validation for the transformation of crystalline metal oxides into amorphous metal glycerolates. Such a transformation effectively enhances the activity of Mn species in facilitating the methanolysis of PET, ultimately yielding monomers.

To directly confirm the formation of *M*-glycerolates on $CaMnO_3$ after the PGM reaction, the reacted $CaMnO_3$ underwent thorough washing with 1,4-dioxane followed by drying. Subsequently, hydrolysis with water was carried out to extract the glycerol and glycerol acetates from the *M*-glycerolates on the catalyst. This hydrolysis process took

https://doi.org/10.1021/jacsau.4c00459
JACS Au 2024, 4, 3135−3145

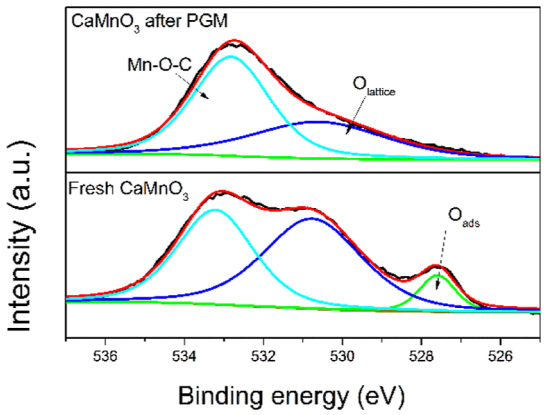

Figure 6. Deconvolution of O 1s spectra of XPS of fresh $CaMnO_3$ and $CaMnO_3$ after the PGM reaction.

place in water at 90 °C for 48 h. The resulting precipitate was filtered, and the solution underwent analysis using gas chromatography−mass spectrometry (GC−MS). Figure S9C−G illustrates the GC spectrum, where a broad peak corresponding to glycerol was identified. Additionally, a smaller peak, attributed to monoacetin, was observed following the glycerol peak. No peaks indicative of diacetin or triacetin were detected in the GC spectra, potentially due to concentrations falling below the GC−MS detection limit. These findings offer robust evidence supporting the formation of *M*-glycerolates on $CaMnO_3$ during the PGM reaction, facilitated by the interaction between metal oxides and glycerol/glycerol acetates.

Based on the discussion above, the possible mechanism of the PGM reaction process by $CaMnO_3$ is illustrated in Scheme 2. First, perovskite-type $CaMnO_3$ serves as a catalyst for the transesterification of glycerol and MA, yielding glycerol acetates and methanol. Concurrently, both glycerol and acetins can bind with Ca and Mn to create catalytic composites composed of amorphous metal-glycerolate encapsulating small $CaMnO_3$ nanoparticles. The presence of Mn-glycerolate may enhance the interaction between Mn and PET/methanol due to the increased affinity. The lone electron pair in the oxygen of the C═O bond from PET is attracted by the Mn^{4+} ion in Mn-glycerolate, facilitating ester bond cleavage. Adjacent to Mn, the Ca atom activates the methanol molecule through O−H bond cleavage, and the lattice oxygen O^- abstracts the H from the hydroxyl group of methanol to form CH_3O^-. This species subsequently associates with the carbon in the ester bonds of PET, leading to chain breakdown into oligomers. Meanwhile, the Ca^{2+} cations can protonate the C═O groups in ester groups of PET, rendering these ester groups more electrophilic and, thus, more susceptible to nucleophilic attack by methanol. This process results in the production of HEMT, which further converts into the DMT monomer.

Finally, in terms of the real application of this tandem reaction system, a crucial challenge is the separation and purification of the products as complex mixtures will be generated. PET monomers can be separated via crystallization by the addition of another solvent. Moreover, the nonvolatile glycerol derivatives can be separated from the solvent and volatile products by distillation. The unreacted feedstocks must be collected for reuse. Our work introduces a promising route for waste co-upcycling, though further investigation will be needed for practical application.

Scheme 2. Proposed Mechanism of *M*-Glycerolate Species Generation and Catalytic PEM Reaction

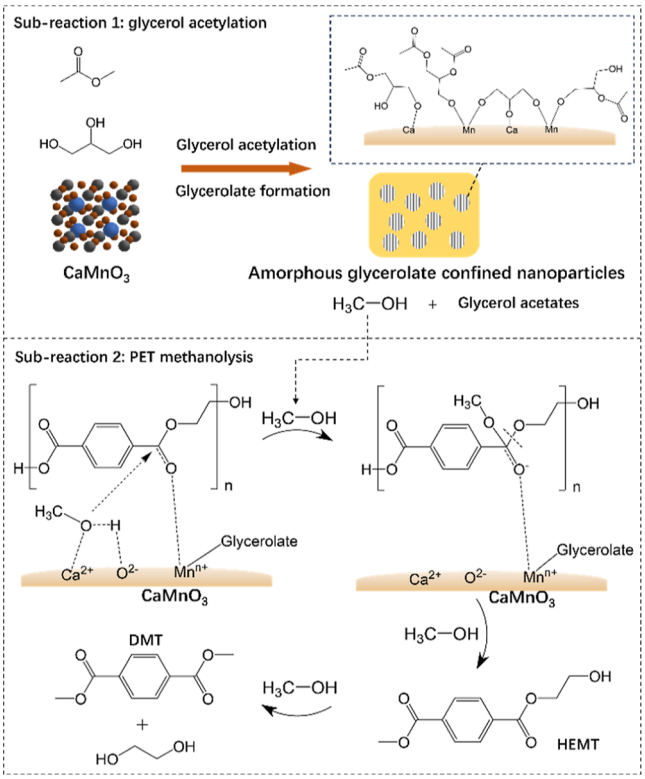

CONCLUSIONS

In this study, we introduce a novel approach for concurrently upgrading three waste feedstocks: PET plastic, biowaste glycerol, and industrial byproduct MA, without requiring any additional feedstock. Through the utilization of coupled tandem transesterification reactions, we accomplish two key subreactions: the acetylation of glycerol into glycerol acetates and the depolymerization of PET into DMT and HEMT, within a single catalytic process. Methanol, generated from the reaction between glycerol and MA, is subsequently consumed in situ by PET methanolysis, optimizing the feedstock efficiency. The selected catalyst, perovskite-structured $CaMnO_3$, demonstrates remarkable versatility in catalyzing the tandem reactions. Notably, the $CaMnO_3$ catalyst undergoes in situ activation during the first reaction, forming amorphous metal-glycerolate flake composites encapsulating $CaMnO_3$ nanoparticles. This generated composite serves as an effective catalyst for the subsequent step of PET depolymerization into monomers. Furthermore, the catalyst exhibited remarkable reusability with a slightly enhanced performance observed over successive reactions, attributed to the in situ generation of new catalytic sites. The Ca and Mn active sites exhibit a synergistic effect, facilitating PET depolymerization. This approach yields over 70% glycerol acetate products and 68% PET monomers at 200 °C for 7 h. This work pioneers a new avenue for the co-upcycling of plastic waste and industrial biowaste with maximized feedstock utilization efficiency, promising economic benefits, and enhanced sustainability. It is anticipated that these findings will inspire further research in this field, driving the development of highly efficient protocols for transforming waste into valuable resources.

https://doi.org/10.1021/jacsau.4c00459
JACS Au 2024, 4, 3135−3145

EXPERIMENTAL SECTION

Chemicals and Materials

All of the chemicals used in this work were purchased from Sigma-Aldrich unless otherwise specified.

Synthesis of Catalysts

CaO and MgO were purchased from Sigma-Aldrich and used without further treatment.

LDH catalysts were prepared via a simple coprecipitation method. The preparation procedure for MgAl-LDH is as follows. A mixed solution of nitrate salts $Mg(NO_3)_2$ and $Al(NO_3)_3$ in 20 mL of deionized water containing 9 mmol of Mg^{2+} and 3 mmol of Al^{3+} was prepared. In a separated container, 19.2 mmol of NaOH and 6 mmol of Na_2CO_3 were dissolved in 40 mL of water to form an alkaline solution. Then the nitrate salt solution was dropwise added into the alkaline solution and the mixture was continuously stirred at room temperature for 3 h. Afterward, the mixture was transferred into a stainless-steel autoclave with a polytetrafluoroethylene (PTFE) liner and aged at 150 °C for 12 h. The precipitate was separated from the solution, repeatedly washed with deionized water several times by centrifugation, and then dried at 80 °C overnight. CaAl-LDH was prepared with the same process, except that $Mg(NO_3)_2$ was replaced by $Ca(NO_3)_2$.

The MnO_x sample was prepared by calcination of 2 g of $Mn(NO_3)_2{\cdot}4H_2O$ at 500 °C for 5 h in static air at a ramping rate of 10 °C/min.

$MgMn_2O_4$ spinel oxides were prepared via the Pechini method as reported elsewhere.[57] 10 mmol of $Mn(NO_3)_2{\cdot}4H_2O$, 5 mmol of $Mg(NO_3)_2{\cdot}6H_2O$, and 30 mmol of citric acid (CA) were dissolved in 10 mL of deionized water while stirring. Then 10 mL of glycol was slowly added into the solution, and the mixture was heated at 70 °C with stirring for approximately 12 h until a brown gel was formed. The gel was transferred to a muffle furnace and calcined at 200 °C, and the resulting solid was further calcined at 450 °C for 12 h in air to eliminate the carbon residual. The obtained $MgMn_2O_4$ spinel oxides were ground into fine powder for further catalytic reactions.

The perovskite-type $CaMnO_3$ oxides were prepared via a sol−gel method. Stoichiometric amounts of calcium and manganese nitrate precursors were dissolved in deionized water. In a separate beaker, ethylenediaminetetraacetic acid (EDTA) and CA were dissolved in ammonium hydroxide. The molar ratio of the total amount of metal ions EDTA and CA was 1:1:2. The solutions were combined with stirring to obtain a transparent solution. Then the solution was heated at 80 °C with stirring until a viscous gel was formed. The gel was heated in a furnace at 250 °C for 5 h. The resulting black ash was further calcined at 1000 °C for 10 h with a ramping rate of 10 °C/min in static air to burn off the remaining organics or nitrates and to form the desired perovskite phase oxides. The solid was ground into fine powder to obtain the $CaMnO_3$ oxide catalyst.

The coprecipitation method for preparation of $CaMnO_3$ was performed by dissolving 5 mmol of calcium and manganese nitrate precursors in 120 mL of water under stirring, followed by the dropwise addition of ammonia solution (30%) until pH = 10. The mixture was kept stirring at room temperature for 12 h, and then the precipitate was filtered out, washed with water, dried at 80 °C, and finally calcined at 1000 °C for 10 h in static air.

For hydrothermal preparation of $CaMnO_3$, 5 mmol of calcium nitrate and 5 mmol of manganese nitrate were dissolved in 60 mL of water, and then 3.3 mmol of cetyltrimethylammonium bromide was added into the solution under stirring. After the mixture became transparent, 13 mL of ammonia solution (30%) was added dropwise and kept stirring for 1 h. Then the mixture was enclosed into a pressurized vessel and kept at 100 °C for 24 h. After filtration and drying, the powder was calcined at 1000 °C for 10 h in static air to obtain the final catalyst.

Catalyst Evaluation

The catalyst evaluation was performed in a stainless-steel autoclave with a PTFE liner. For example, in a typical tandem transesterification reaction of glycerol, MA, and PET, 10 mmol of glycerol, 30 mmol of MA, 2 mL of 1,4-dioxane, 0.05 g of PET film, and 1.8 mmol of metal catalyst were loaded into an autoclave reactor. The autoclave reactor was purged with argon, sealed, and heated at the target temperature in an oil bath under magnetic stirring for 7 h. The reaction was carried out under autogenous pressure (with an initial argon pressure of 1 atm). After the reaction was finished, the reactor was cooled to room temperature and 0.15 mmol of anisole was loaded into the mixture as the internal standard. Excessive 1,4-dioxane solvent was added to the reaction mixture to fully dissolve the products and dilute the solution. The solid catalyst was filtered. The product in the solvent was analyzed by gas chromatography−mass spectrometry (GCMS) on an Agilent 7890B GC system and a 5977A MSD detector, equipped with an HP-5MS column.

The products were quantified by the calibrated peak area of GCMS. The reaction efficiency of the glycerol acetylation and PET methanolysis reactions was reflected by the yield of mono-, di-, and triacetin and DMT and HEMT, respectively. The product yield of mono-, di-, and triacetin was calculated using the following equation

$$\text{yield} = \frac{\text{mole of glycerol acetate}}{\text{mole of initial glycerol}} \times 100\%$$

The product yield of DMT and HEMT was calculated using the following equation

$$\text{yield} = \frac{\text{mole of DMT or HEMT} \times 192.16\text{g/mol}}{\text{mass of initial PET (g)}} \times 100\%$$

For mass and carbon balance calculations, high-performance liquid chromatography (HPLC) with a refractive index detector (RID) was employed to quantify the methanol and EG after the reaction. The total mass of PET oligomers and monomers was determined by evaporating the volatile solvent and products and washing off the glycerol/acetins with water. The remaining precipitate was dried and weighed to calculate the oligomers.

Characterization

SEM and TEM images were obtained on Zeiss Sigma HD FEG SEM and JEOL 2200FS TEM equipment, respectively. The sample powder was dispersed on carbon tape and coated with 5 nm thick Au prior to imaging. XPS measurements were conducted by utilizing a Thermo Fisher ESCALAB 250Xi spectrometer, employing monochromatic Al Kα-rays (1486.6 eV) as the radiation source. The data peak fitting was performed by using XPSPEAK41 software. XRD patterns were obtained on a Rigaku Smartlab SE powder diffractometer equipped with a Cu Kα X-ray source operating at 40 kV and 40 mA. TGA was performed on a Jupiter STA 449 F3 instrument. In each experiment, 10 mg of the sample was loaded into the instrument under an air environment and heated from 40 to 800 °C with a ramping rate of 10 °C/min and a gas flow rate of 30 mL/min. FTIR spectroscopy was performed on a Nicolet iS5 FTIR spectrophotometer with an attenuated total reflectance (ATR) accessory (iD5). The N_2 adsorption and desorption isotherms were performed on a Tristar II 3020 instrument (Micromeritics) in a liquid nitrogen environment to determine the SSA of $CaMnO_3$ samples using the Brunauer−Emmett−Teller (BET) method. ICP-OES was conducted on a PerkinElmer Avio 500 instrument.

ASSOCIATED CONTENT

Supporting Information

The Supporting Information is available free of charge at https://pubs.acs.org/doi/10.1021/jacsau.4c00459.

Catalytic reaction performance and characterization results including XRD, FTIR, XPS, and GC−MS (PDF)

https://doi.org/10.1021/jacsau.4c00459
JACS Au 2024, 4, 3135−3145

AUTHOR INFORMATION

Corresponding Authors

Jun Huang − *School of Chemical and Biomolecular Engineering, Sydney Nano Institute, The University of Sydney, Sydney, New South Wales 2037, Australia;* orcid.org/0000-0001-8704-605X; Email: jun.huang@sydney.edu.au

Yijiao Jiang − *School of Engineering, Macquarie University, Sydney, New South Wales 2109, Australia;* orcid.org/0000-0002-6191-9825; Email: yijiao.jiang@mq.edu.au

Authors

Jiaquan Li − *School of Chemical and Biomolecular Engineering, Sydney Nano Institute, The University of Sydney, Sydney, New South Wales 2037, Australia; School of Engineering, Macquarie University, Sydney, New South Wales 2109, Australia;* orcid.org/0000-0001-7924-0573

Xingmo Zhang − *School of Chemical and Biomolecular Engineering, Sydney Nano Institute, The University of Sydney, Sydney, New South Wales 2037, Australia;* orcid.org/0000-0003-2147-2069

Xingxu Liu − *School of Chemical and Biomolecular Engineering, Sydney Nano Institute, The University of Sydney, Sydney, New South Wales 2037, Australia*

Xiuping Liao − *School of Engineering, Macquarie University, Sydney, New South Wales 2109, Australia*

Complete contact information is available at: https://pubs.acs.org/10.1021/jacsau.4c00459

Author Contributions

Jiaquan Li: Conceptualization, Investigation, Formal analysis, Methodology, Writing−original draft; Xingmo Zhang: Investigation. Xingxu Liu, Investigation. Xiuping Liao, Investigation. Jun Huang: Supervision, Conceptualization, Resources, Writing—Review and Editing. Yijiao Jiang: Resources, Writing—Review and Editing. CRediT: **Jiaquan Li** conceptualization, formal analysis, investigation, methodology, writing-original draft; **Xingmo Zhang** investigation; **Xingxu Liu** investigation; **Xiuping Liao** investigation; **Jun Huang** conceptualization, resources, supervision, writing-review & editing; **Yijiao Jiang** resources, writing-review & editing.

Notes

The authors declare no competing financial interest.

ACKNOWLEDGMENTS

This work was supported by the Australia Research Council Discovery Project (DP22002851) and Future Fellowship (FT220100601). This research was facilitated by access to Sydney Microscopy & Microanalysis and Sydney Analytical at the University of Sydney.

REFERENCES

(1) Zhao, X.; Boruah, B.; Chin, K. F.; Đokić, M.; Modak, J. M.; Soo, H. S. Upcycling to Sustainably Reuse Plastics. *Adv. Mater.* **2022**, *34*, 2100843.

(2) Zhang, M.-Q.; Wang, M.; Sun, B.; Hu, C.; Xiao, D.; Ma, D. Catalytic strategies for upvaluing plastic wastes. *Chem.* **2022**, *8*, 2912−2923.

(3) Naderi Kalali, E.; Lotfian, S.; Entezar Shabestari, M.; Khayatzadeh, S.; Zhao, C.; Yazdani Nezhad, H. A critical review of the current progress of plastic waste recycling technology in structural materials. *Curr. Opin. Green Sustainable Chem.* **2023**, *40*, 100763.

(4) Chen, H.; Wan, K.; Zhang, Y.; Wang, Y. Waste to Wealth: Chemical Recycling and Chemical Upcycling of Waste Plastics for a Great Future. *ChemSusChem* **2021**, *14*, 4123−4136.

(5) Raheem, A. B.; Noor, Z. Z.; Hassan, A.; Abd Hamid, M. K.; Samsudin, S. A.; Sabeen, A. H. Current developments in chemical recycling of post-consumer polyethylene terephthalate wastes for new materials production: A review. *J. Cleaner Prod.* **2019**, *225*, 1052−1064.

(6) Zhang, S.; Li, M.; Zuo, Z.; Niu, Z. Recent advances in plastic recycling and upgrading under mild conditions. *Green Chem.* **2023**, *25*, 6949−6970.

(7) Westhues, S.; Idel, J.; Klankermayer, J. Molecular catalyst systems as key enablers for tailored polyesters and polycarbonate recycling concepts. *Sci. Adv.* **2018**, *4*, No. eaat9669.

(8) Kratish, Y.; Li, J.; Liu, S.; Gao, Y.; Marks, T. J. Polyethylene Terephthalate Deconstruction Catalyzed by a Carbon-Supported Single-Site Molybdenum-Dioxo Complex. *Angew. Chem., Int. Ed.* **2020**, *59*, 19857−19861.

(9) Jing, Y.; Wang, Y.; Furukawa, S.; Xia, J.; Sun, C.; Hülsey, M. J.; Wang, H.; Guo, Y.; Liu, X.; Yan, N. Towards the Circular Economy: Converting Aromatic Plastic Waste Back to Arenes over a Ru/Nb_2O_5 Catalyst. *Angew. Chem., Int. Ed.* **2021**, *60*, 5527−5535.

(10) Liu, Y.; Yao, X.; Yao, H.; Zhou, Q.; Xin, J.; Lu, X.; Zhang, S. Degradation of poly(ethylene terephthalate) catalyzed by metal-free choline-based ionic liquids. *Green Chem.* **2020**, *22*, 3122−3131.

(11) Zhang, S.; Xue, Y.; Wu, Y.; Zhang, Y.-X.; Tan, T.; Niu, Z. PET recycling under mild conditions via substituent-modulated intramolecular hydrolysis. *Chem. Sci.* **2023**, *14*, 6558−6563.

(12) Maqsood, T.; Dai, J.; Zhang, Y.; Guang, M.; Li, B. Pyrolysis of plastic species: A review of resources and products. *J. Anal. Appl. Pyrolysis* **2021**, *159*, 105295.

(13) Uekert, T.; Kuehnel, M. F.; Wakerley, D. W.; Reisner, E. Plastic waste as a feedstock for solar-driven H_2 generation. *Energy Environ. Sci.* **2018**, *11*, 2853−2857.

(14) Uekert, T.; Kasap, H.; Reisner, E. Photoreforming of Nonrecyclable Plastic Waste over a Carbon Nitride/Nickel Phosphide Catalyst. *J. Am. Chem. Soc.* **2019**, *141*, 15201−15210.

(15) Wang, J.; Li, X.; Wang, M.; Zhang, T.; Chai, X.; Lu, J.; Wang, T.; Zhao, Y.; Ma, D. Electrocatalytic Valorization of Poly(ethylene terephthalate) Plastic and CO_2 for Simultaneous Production of Formic Acid. *ACS Catal.* **2022**, *12*, 6722−6728.

(16) Li, Y.; Wang, M.; Liu, X.; Hu, C.; Xiao, D.; Ma, D. Catalytic Transformation of PET and CO_2 into High-Value Chemicals. *Angew. Chem., Int. Ed.* **2022**, *61*, No. e202117205.

(17) Liang, X.; Wang, M.; Ma, D. One-Pot Conversion of Polyester and Carbonate into Formate without External H_2. *J. Am. Chem. Soc.* **2024**, *146*, 2711−2717.

(18) Tang, H.; Li, N.; Li, G.; Wang, A.; Cong, Y.; Xu, G.; Wang, X.; Zhang, T. Synthesis of gasoline and jet fuel range cycloalkanes and aromatics from poly(ethylene terephthalate) waste. *Green Chem.* **2019**, *21*, 2709−2719.

(19) Li, M.; Zhang, S. Coupling Waste Plastic Upgrading and CO2 Photoreduction to High-Value Chemicals by a Binuclear Re−Ru Heterogeneous Catalyst. *ACS Catal.* **2024**, *14*, 6717−6727.

(20) Tollini, F.; Brivio, L.; Innocenti, P.; Sponchioni, M.; Moscatelli, D. Influence of the catalytic system on the methanolysis of polyethylene terephthalate at mild conditions: A systematic investigation. *Chem. Eng. Sci.* **2022**, *260*, 117875.

(21) Cheng, X.; Dong, S.; Chen, D.; Rui, Q.; Guo, J.; Dayong, W.; Jiang, J. Potential of esterase DmtH in transforming plastic additive dimethyl terephthalate to less toxic mono-methyl terephthalate. *Ecotoxicol. Environ. Saf.* **2020**, *187*, 109848.

(22) Pham, D. D.; Cho, J. Low-energy catalytic methanolysis of poly(ethyleneterephthalate). *Green Chem.* **2021**, *23*, 511−525.

(23) Genta, M.; Iwaya, T.; Sasaki, M.; Goto, M.; Hirose, T. Depolymerization Mechanism of Poly(ethylene terephthalate) in Supercritical Methanol. *Ind. Eng. Chem. Res.* **2005**, *44*, 3894−3900.

(24) Yang, Y.; Lu, Y.; Xiang, H.; Xu, Y.; Li, Y. Study on methanolytic depolymerization of PET with supercritical methanol for chemical recycling. *Polym. Degrad. Stab.* **2002**, *75*, 185−191.
(25) Du, J.-T.; Sun, Q.; Zeng, X.-F.; Wang, D.; Wang, J.-X.; Chen, J.-F. ZnO nanodispersion as pseudohomogeneous catalyst for alcoholysis of polyethylene terephthalate. *Chem. Eng. Sci.* **2020**, *220*, 115642.
(26) Mishra, S.; Goje, A. S. Kinetic and thermodynamic study of methanolysis of poly(ethylene terephthalate) waste powder. *Polym. Int.* **2003**, *52*, 337−342.
(27) Laldinpuii, Z. T.; Khiangte, V.; Lalhmangaihzuala, S.; Lalmuanpuia, C.; Pachuau, Z.; Lalhriatpuia, C.; Vanlaldinpuia, K. Methanolysis of PET Waste Using Heterogeneous Catalyst of Biowaste Origin. *J. Polym. Environ.* **2022**, *30*, 1600−1614.
(28) Ma, M.; Wang, S.; Liu, Y.; Yu, H.; Yu, S.; Ji, C.; Li, H.; Nie, G.; Liu, S. Insights into the depolymerization of polyethylene terephthalate in methanol. *J. Appl. Polym. Sci.* **2022**, *139*, No. e52814.
(29) Sun, Q.; Zheng, Y.-Y.; Yun, L.-X.; Wu, H.; Liu, R.-K.; Du, J.-T.; Gu, Y.-H.; Shen, Z.-G.; Wang, J.-X. Fe3O4 Nanodispersions as Efficient and Recoverable Magnetic Nanocatalysts for Sustainable PET Glycolysis. *ACS Sustainable Chem. Eng.* **2023**, *11*, 7586−7595.
(30) Park, G.; Bartolome, L.; Lee, K. G.; Lee, S. J.; Kim, D. H.; Park, T. J. One-step sonochemical synthesis of a graphene oxide−manganese oxide nanocomposite for catalytic glycolysis of poly(ethylene terephthalate). *Nanoscale* **2012**, *4*, 3879−3885.
(31) Zhang, S.; Hu, Q.; Zhang, Y.-X.; Guo, H.; Wu, Y.; Sun, M.; Zhu, X.; Zhang, J.; Gong, S.; Liu, P.; Niu, Z. Depolymerization of polyesters by a binuclear catalyst for plastic recycling. *Nat Sustainability* **2023**, *6*, 965−973.
(32) Li, M.; Zhang, S. Tandem Chemical Depolymerization and Photoreforming of Waste PET Plastic to High-Value-Added Chemicals. *ACS Catal.* **2024**, *14*, 2949−2958.
(33) Gupta, M.; Kumar, N. Scope and opportunities of using glycerol as an energy source. *Renewable Sustainable Energy Rev.* **2012**, *16*, 4551−4556.
(34) Lima, P. J. M.; da Silva, R. M.; Neto, C. A. C. G.; Gomes e Silva, N. C.; Souza, J. E. d.S.; Nunes, Y. L.; Sousa dos Santos, J. C. An overview on the conversion of glycerol to value-added industrial products via chemical and biochemical routes. *Biotechnol. Appl. Biochem.* **2022**, *69*, 2794−2818.
(35) Al-Saadi, L. S.; Eze, V. C.; Harvey, A. P. Techno-Economic Analysis of Glycerol Valorization via Catalytic Applications of Sulphonic Acid-Functionalized Copolymer Beads. *Front. Chem.* **2020**, *7*, 882.
(36) Rigo, D.; Polidoro, D.; Marcuzzo, L.; Perosa, A.; Selva, M. Isopropenyl Acetate for the Continuous-Flow Synthesis of Triacetin, Solketal Acetate, and Allyl Acetate from Pure or Crude Glycerol. *ACS Sustainable Chem. Eng.* **2023**, *11*, 12602−12613.
(37) Shafiei, A.; Rastegari, H.; Ghaziaskar, H. S.; Yalpani, M. Glycerol transesterification with ethyl acetate to synthesize acetins using ethyl acetate as reactant and entrainer. *Biofuel Res. J.* **2017**, *4*, 565−570.
(38) Patel, A.; Singh, S. A green and sustainable approach for esterification of glycerol using 12-tungstophosphoric acid anchored to different supports: Kinetics and effect of support. *Fuel* **2014**, *118*, 358−364.
(39) Sánchez, J. A.; Hernández, D. L.; Moreno, J. A.; Mondragón, F.; Fernández, J. J. Alternative carbon based acid catalyst for selective esterification of glycerol to acetylglycerols. *Appl. Catal., A* **2011**, *405*, 55−60.
(40) Liao, X.; Zhu, Y.; Wang, S.-G.; Li, Y. Producing triacetylglycerol with glycerol by two steps: Esterification and acetylation. *Fuel Process. Technol.* **2009**, *90*, 988−993.
(41) Fortunatti Montoya, M.; Sánchez, F. A.; Hegel, P. E.; Pereda, S. Phase equilibrium engineering of glycerol acetates fractionation with pressurized CO_2. *J. Supercrit. Fluids* **2018**, *132*, 51−64.
(42) Vargas, B. J.; Menezes Vicenti, J. R. d.; Silva, E. D. d.; Pinto, A. H.; Gorup, L. F.; Rosa, C. A. d.; Mortola, V. B. Glycerol valorization: The effect of Cu on the HZSM5 catalyst structure and increased selectivity towards allyl alcohol. *Chem. Eng. Res. Des.* **2023**, *196*, 617−631.
(43) Pandit, K.; Jeffrey, C.; Keogh, J.; Tiwari, M. S.; Artioli, N.; Manyar, H. G. Techno-Economic Assessment and Sensitivity Analysis of Glycerol Valorization to Biofuel Additives via Esterification. *Ind. Eng. Chem. Res.* **2023**, *62*, 9201−9210.
(44) Zhang, Q.; Cui, X.; Feng, T.; Zhang, Y.; Zhang, X.; He, J.; Wang, J. Hydrolysis of methyl acetate using ionic liquids as catalyst and solvent. *Mol. Catal.* **2020**, *484*, 110785.
(45) Morales, G.; Paniagua, M.; Melero, J. A.; Vicente, G.; Ochoa, C. Sulfonic Acid-Functionalized Catalysts for the Valorization of Glycerol via Transesterification with Methyl Acetate. *Ind. Eng. Chem. Res.* **2011**, *50*, 5898−5906.
(46) Khayoon, M. S.; Hameed, B. H. Yttrium-grafted mesostructured SBA-3 catalyst for the transesterification of glycerol with methyl acetate to synthesize fuel oxygenates. *Appl. Catal., A* **2013**, *460*−*461*, 61−69.
(47) Oh, S.; Park, C. Enzymatic production of glycerol acetate from glycerol. *Enzyme Microb. Technol.* **2015**, *69*, 19−23.
(48) Chiao, Y.-W.; Liao, W.; Krisbiantoro, P. A.; Yu, B.-Y.; Wu, K. C. W. Waste-battery-derived multifunctional zinc catalysts for glycolysis and decolorization of polyethylene terephthalate. *Appl. Catal. B: Environ.* **2023**, *325*, 122302.
(49) Gonçalves, J. M.; Hennemann, A. L.; Ruiz-Montoya, J. G.; Martins, P. R.; Araki, K.; Angnes, L.; Shahbazian-Yassar, R. Metal-glycerolates and their derivatives as electrode materials: A review on recent developments, challenges, and future perspectives. *Coord. Chem. Rev.* **2023**, *477*, 214954.
(50) Zhang, G.; Wu, H. B.; Hoster, H. E.; Lou, X. W. Strongly coupled carbon nanofiber−metal oxide coaxial nanocables with enhanced lithium storage properties. *Energy Environ. Sci.* **2014**, *7*, 302−305.
(51) Liu, X.; Gong, M.; Deng, S.; Zhao, T.; Zhang, J.; Wang, D. Recent advances on metal alkoxide-based electrocatalysts for water splitting. *J. Mater. Chem. A* **2020**, *8*, 10130−10149.
(52) Prégent, J.; Vandsburger, L.; Blanchard, V.; Blanchet, P.; Riedl, B.; Sarkissian, A.; Stafford, L. Determination of active species in the modification of hardwood samples in the flowing afterglow of N_2 dielectric barrier discharges open to ambient air. *Cellulose* **2015**, *22*, 811−827.
(53) Khonina, T. G.; Nikitina, E. Y.; Germov, A. Y.; Goloborodsky, B. Y.; Mikhalev, K. N.; Bogdanova, E. A.; Tishin, D. S.; Demin, A. M.; Krasnov, V. P.; Chupakhin, O. N.; Charushin, V. N. Individual iron(iii) glycerolate: synthesis and characterisation. *RSC Adv.* **2022**, *12*, 4042−4046.
(54) Du, J.; Zhang, T.; Cheng, F.; Chu, W.; Wu, Z.; Chen, J. Nonstoichiometric Perovskite $CaMnO_{3-\delta}$ for Oxygen Electrocatalysis with High Activity. *Inorg. Chem.* **2014**, *53*, 9106−9114.
(55) Han, X.; Hu, Y.; Yang, J.; Cheng, F.; Chen, J. Porous perovskite $CaMnO_3$ as an electrocatalyst for rechargeable Li−O_2 batteries. *Chem. Commun.* **2014**, *50*, 1497−1499.
(56) Chang, L.; Li, J.; Le, Z.; Nie, P.; Guo, Y.; Wang, H.; Xu, T.; Xue, X. Perovskite-type $CaMnO_3$ anode material for highly efficient and stable lithium ion storage. *J. Colloid Interface Sci.* **2021**, *584*, 698−705.
(57) Yokozaki, R.; Kobayashi, H.; Mandai, T.; Honma, I. Effect of Al substitution on structure and cathode performance of $MgMn_2O_4$ spinel for magnesium rechargeable battery. *J. Alloys Compd.* **2021**, *872*, 159723.

https://doi.org/10.1021/jacsau.4c00459
JACS Au 2024, 4, 3135−3145